

Analysis of the fluid-structure interaction transient process of spent fuel storage rack based on POD and DMD

Fei Zhao¹, Daogang Lu², Yuchao Wang³, Yu Liu^{4*}

¹ Mr., North China Electric Power University, Beijing

² Prof., North China Electric Power University, Beijing

³ Mr., North China Electric Power University, Beijing

⁴ Dr., North China Electric Power University, Beijing (appleplanter@ncepu.edu.cn)

ABSTRACT

There are many racks in spent fuel pools and reprocessing plants. When analyzing their seismic behavior, it is important to consider how the racks interact with each other and with the pool walls. The flow field in this scenario is complex and difficult to analyze because of the porous structure of the racks and their large quantity. Therefore, the fluid-structure coupling effect is often simplified into added mass and damping for seismic analysis. When calculating added mass and damping, the frequency of the flow field vibration is a crucial parameter. A fast and accurate method is required to isolate the primary frequency of fluid-structure interaction. In this paper, Proper Orthogonal Decomposition (POD) and Dynamic Mode Decomposition (DMD) methods are used to decompose the fluid field into different modes in frequency. A two-dimensional numerical model of a rack is applied. Fluid flows in through the inlet, through the rack, and out through the outlet. Based on the results of the Computational Fluid Dynamics (CFD) simulation, Dynamic Mode Decomposition (DMD) proves to be more effective in decomposing the flow field compared to the Proper Orthogonal Decomposition (POD) method.

INTRODUCTION

In nuclear power plants, there are storage racks immersed in water that hold radioactive spent fuel assemblies. These racks are affected by strong fluid-structure interactions during an earthquake, which makes it difficult to conduct a seismic analysis. However, the seismic analysis is crucial for ensuring the safety of nuclear plants. As a result, there have been studies conducted on the fluid-structure interactions and seismic analysis of these racks. Stabel et.al. (Ren and Stabel, 1999) carried out research on the formula for the coupling between fluid and solid in spent fuel storage racks. The research focused on studying the differences between the fluid force and the analytical solution of added mass in three models: two-dimensional coaxial cylinder, coaxial square tube, and three-dimensional quadrangular prism, based on the analytical solution formula of added mass. Miguel et.al. (Moreira and Antunes, 2002) have developed a theoretical model that can calculate the fluid-structure interaction effect of spent nuclear fuel racks. However, this model makes some simplifying assumptions. It ignores three-dimensional flow effects and assumes that the gaps between fuel assemblies and the container are small compared to the longitudinal length scale. The method describes the gap average velocity and pressure fields in terms of a single spatial coordinate for each fluid channel. Using this method, the flow can be expressed in analytical terms, and the dynamic response of multi-frame fluid-structure interaction systems can be efficiently calculated. Liu Yu (Liu et al., 2017) simplified the side walls of the rack into two parallel plates and studied the fluid-structure interaction characteristics of the fluid between racks and racks and pool walls. Set up an experimental bench and measure the fluid force of the interstitial fluid in the orifice plate under different excitation frequencies and different gap conditions through vibration experiments. The experiment finally gives the fluid force of the gap fluid in the orifice plate and gives the added mass under different gap conditions. Experimental results show that the added mass of the orifice plate is much smaller than that of the flat plate. It is proved that the spent fuel storage rack is designed with a storage cavity with gaps, and the additional mass of the rack using a flat plate is too conservative. The above studies have found that the additional mass and additional damping of the grid vibration are related to the vibration frequency. To accurately calculate the parameters of added mass

and damping in the racks, we need to consider the frequency of fluid vibrations. In our paper, we utilized the DMD and POD methods to decompose the fluid flow field, which helped to determine the added mass and damping frequency.

THE NUMERICAL MODEL

Models and Meshes

The spent fuel storage rack is designed with a pipe end connection and each storage cavity is connected with reinforcing blocks. It is then welded to the bottom plate of the rack to enhance its overall stiffness. (Liu et al., 2017). Neutron-absorbing material is installed on the walls of the storage cavities, along with a circular plate welded to the top of the rack to strengthen its mechanical performance. This helps protect the neutron-absorbing plates from damage. The design allows fluid to flow freely inside and outside the rack, promoting the flow of coolant and reducing the influence of fluid-structure interaction. The rack's bottom plate is supported by four legs, with leveling bolts and pads installed at the bottom of each leg. This design allows the rack to slide freely in the spent fuel pool, eliminating stress between the legs and the pool wall. The rack is immersed in the spent fuel pool up to a depth of 13 meters in a free-standing manner and is not fixed to the adjacent pool wall. The design drawing of the spent fuel storage rack is shown in Figure 1.a. According to the racks model, select the cross section perpendicular to the Z axis and divide it into a two-dimensional mesh, as shown in Figure 1.b.

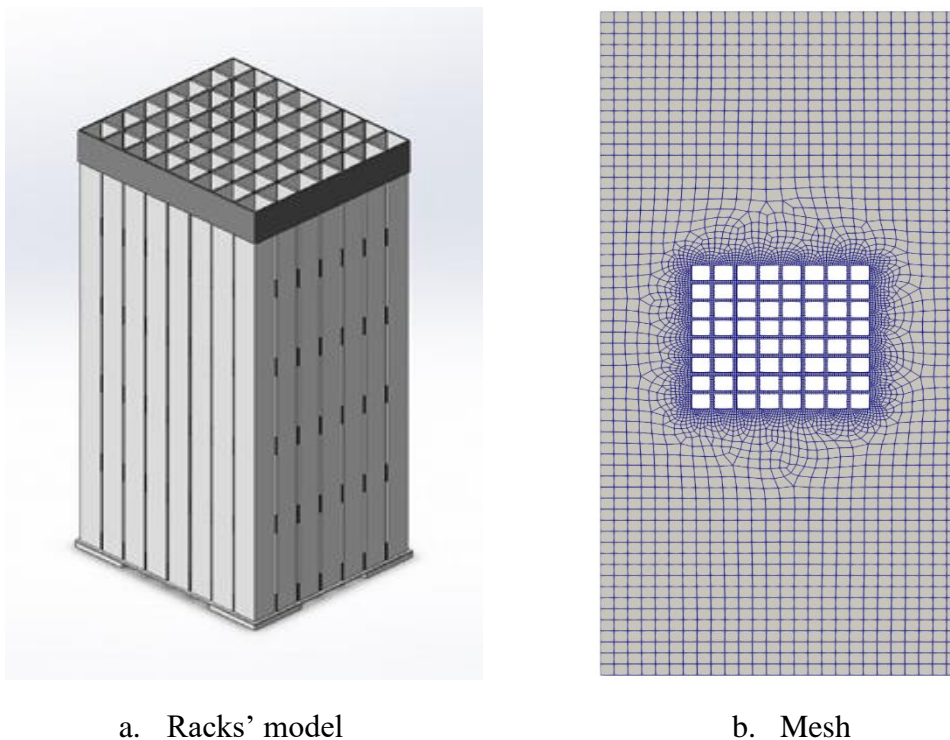


Figure 1 Racks model and mesh

This article utilizes OpenFOAM for calculation, employs the PISO algorithm, and sets the time step to $1E-4$. The kinematic viscosity is set to $1E-6$, using the second-order upwind scheme. The fluid enters from the bottom, passes through the rack, and exits from the top. The inlet has a speed of 1 m/s, whereas the outlet has a pressure of 0 Pa.

DMD model

DMD is an algorithm that uses singular value decomposition (SVD) to analyze the linear dynamics of nonlinear dynamic systems. It identifies the main dynamic modes of a system and represents these modes as exponentials with complex frequencies and growth rates.

Suppose there is a set of time series data $\{X_1, X_2, X_3, \dots, X_n\}$, where $X_1 \in R^n$
 Construct data matrices

$$X = [X_1, X_2, X_3, \dots, X_{m-1}] \quad (1)$$

$$X' = [X_2, X_3, \dots, X_m] \quad (2)$$

Perform Singular Value Decomposition on X

$$[U, S, V] = svd(X) \quad (3)$$

Define matrix A representing the system's linear dynamics.

$$A = U^* \cdot X' \cdot V \cdot S^{-1} \quad (4)$$

Compute eigenvalues and eigenvectors of matrix A; these eigenvectors are the DMD modes.

$$[\omega, \lambda] = eig(A) \quad (5)$$

Calculate DMD modes.

$$\phi = U \cdot \omega \quad (6)$$

$$\phi = X' \cdot V \cdot S^{-1} \cdot \omega \quad (7)$$

Calculate the initial value b corresponding to the DMD mode. The first step is equivalent to the initial value of the signal X_1 .

$$\phi \cdot b = X_1 \quad (8)$$

Sort the modes by their energy. The energy of a mode is defined as the sum of the squares of the amplitudes at each moment. The signal at each moment is equal to the initial signal multiplied by the characteristic value, which can be calculated as:

$$X_k = X_1 \times \phi \times b \times \lambda^{k-1} \quad (9)$$

POD model

Select time series data to form a matrix

$$X = [X_1, X_2, X_3, \dots, X_m] \quad (10)$$

First create the covariance matrix R

$$R = 1/N \cdot (X^* \cdot X) \quad (11)$$

Then perform eigenvalue and eigenvector decomposition, V is the eigenvector, and D is the eigenroot:

$$R \cdot V = D \cdot V \quad (12)$$

The eigenvector is the POD mode we obtained, the energy value of each mode corresponding to the eigenroot, and we also focus on the mode corresponding to the large eigenroot. Generally, the mode corresponding to the largest eigenroot is called the first mode.

$$V = [\phi_1 \phi_2 \phi_3 \dots \phi_m] \quad (13)$$

The amplitude and size of the mode can be expressed by $AA = U \cdot V$

$$A_i = U \cdot \phi_i \quad (14)$$

In this way, we successfully split a time and space signal into the product of two independent time signals and space signals, each i representing a mode.

$$X(t, x) = i = \sum_{i=1}^m A_i(t) \cdot \phi_i(x) \quad (15)$$

After the data obtained from the above CFD calculation is formatted and output as one-dimensional data, it is used as the constituting X matrix for POD and DMD decomposition.

RESULTS AND DISCUSSION

Results of CFD

According to CFD calculation, results can be obtained. The velocity field data from 0.01 seconds to 20s, select the Velocity field data at 0.01s and 10s for display, as shown in Figure 1.

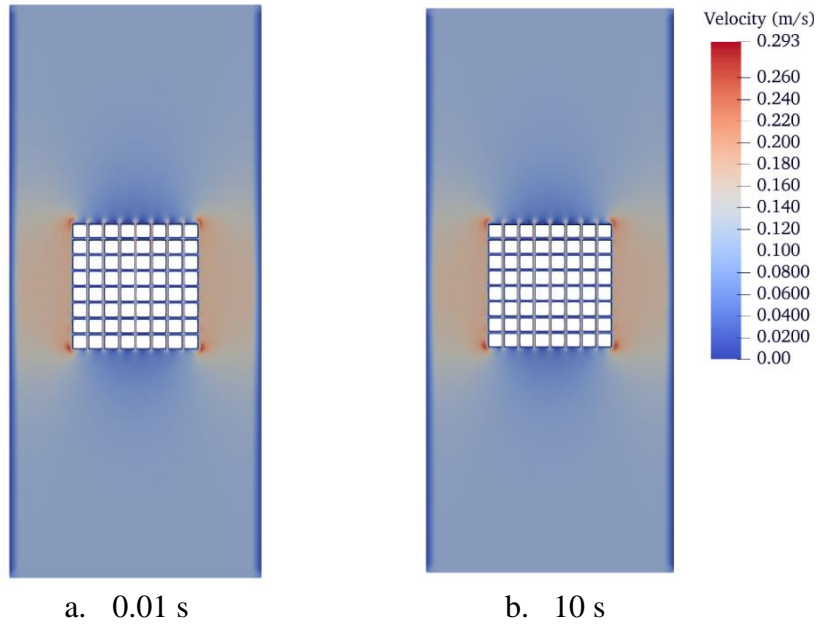


Figure 2 The velocity field

It can be found that the vortex shedding phenomenon occurred after 10 seconds, and the flow field flowing through the grid was muddled.

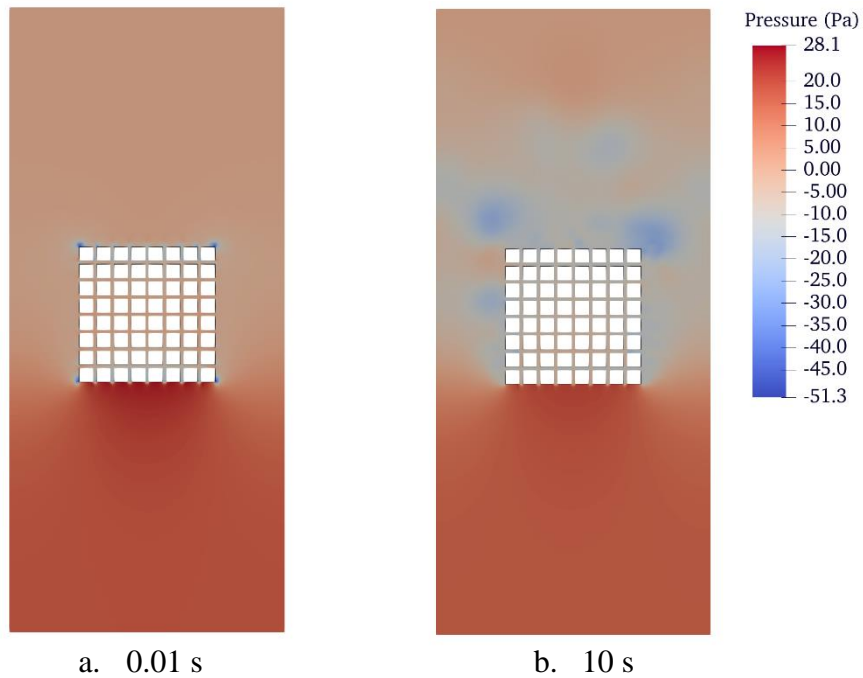


Figure 3 The pressure field

It can be found in Figure 3 that at 10 seconds, low pressure areas of different sizes have occurred, which means that vortices of different sizes have appeared.

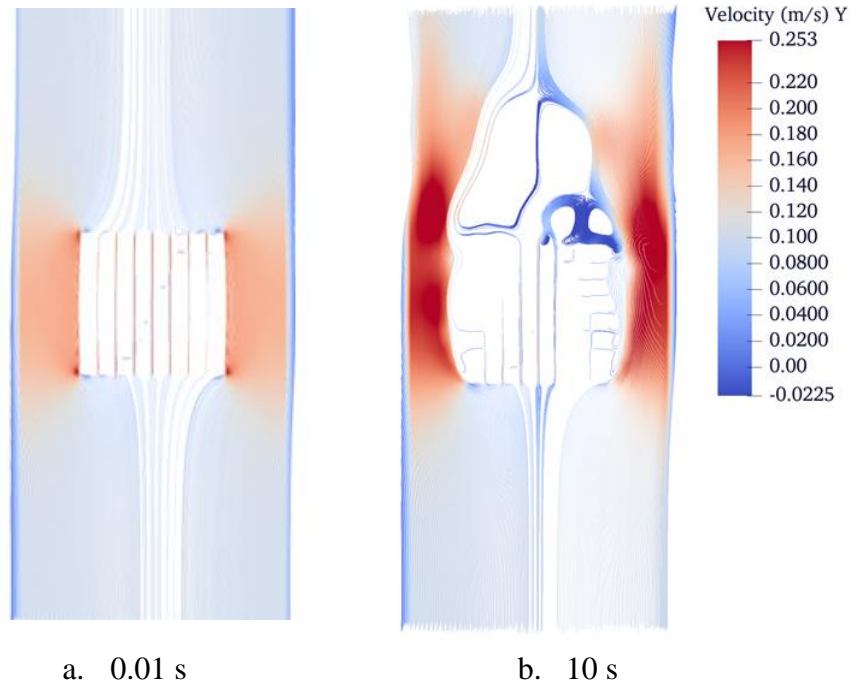


Figure 4 The stream figure

It can be clearly seen in the streamline diagram in Figure 4 that the phenomenon of vortex shedding has occurred.

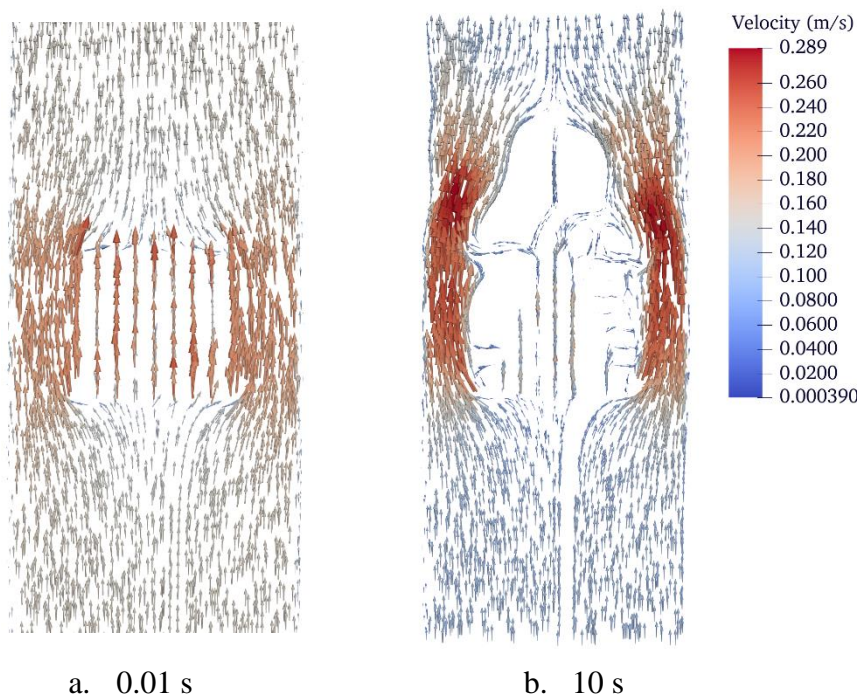


Figure 5 The velocity vector

The velocity vector (Figure 5) also shows the same phenomenon.

Results of DMD

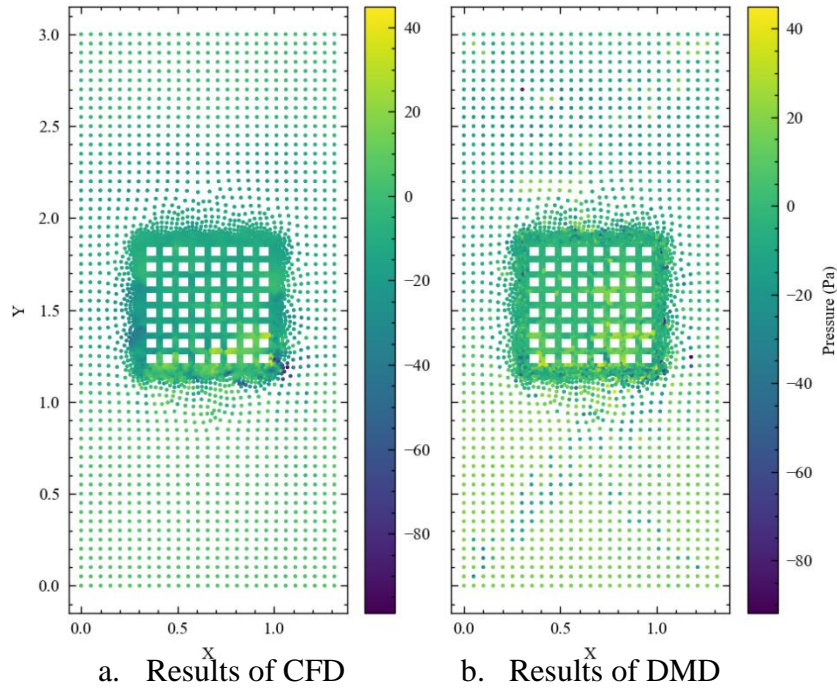


Figure 6 Pressure field decomposed by DMD($t=10$ s)

After DMD decomposition of the pressure field data, the first 7 modes are reconstructed to obtain the pressure field data at each moment. Comparing the results at 10s, it can be found that the accuracy of the first 7 modes is sufficient, as shown in Figure 6.

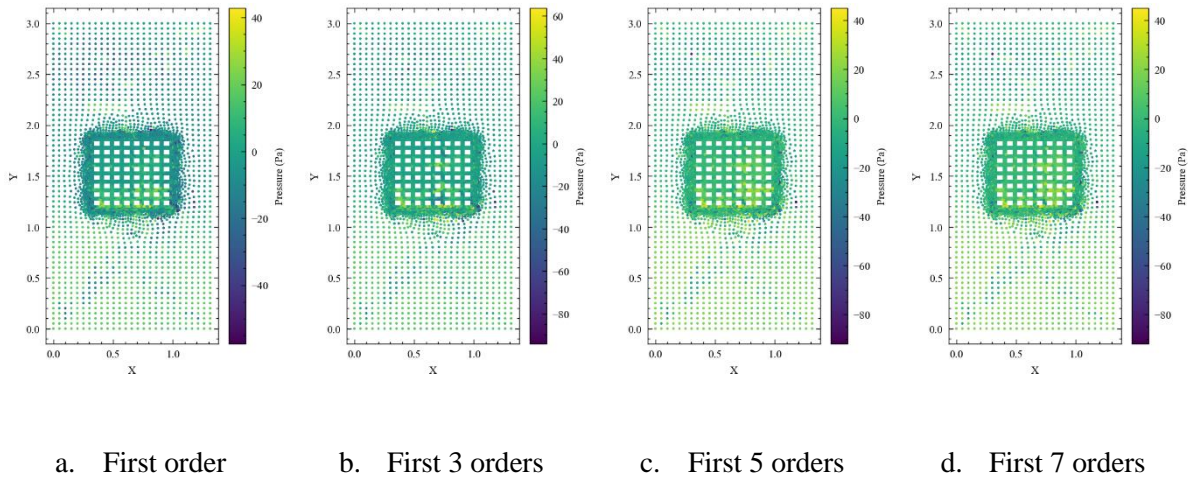


Figure 7 Pressure field reconstructed using different orders ($t=10$ s)

Figure 7 shows the pressure field reconstructed at different orders. It is found that as the order increases, it is closer to the CFD simulation value.

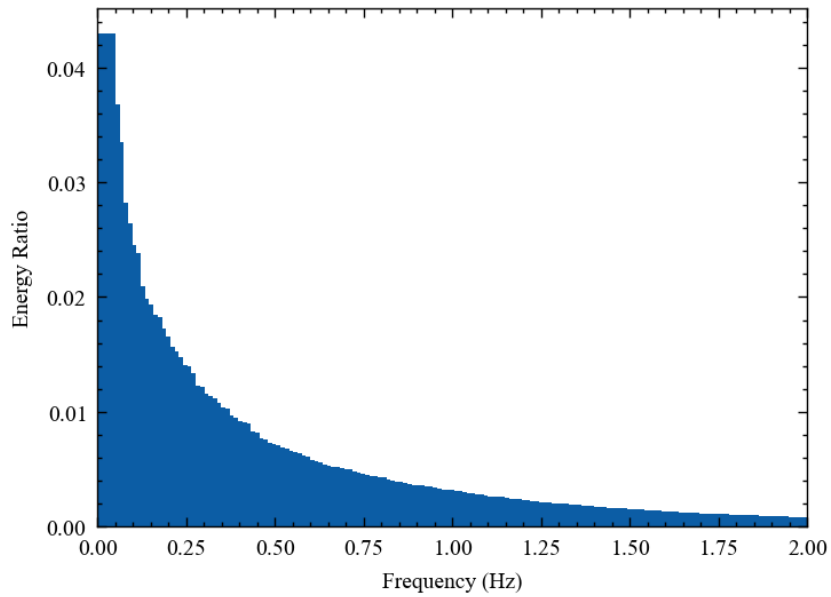


Figure 8 The proportion of energy each frequency by DMD

Figure 8 shows the proportion of energy each frequency. It can be found that the main energy is mostly concentrated below 2Hz.

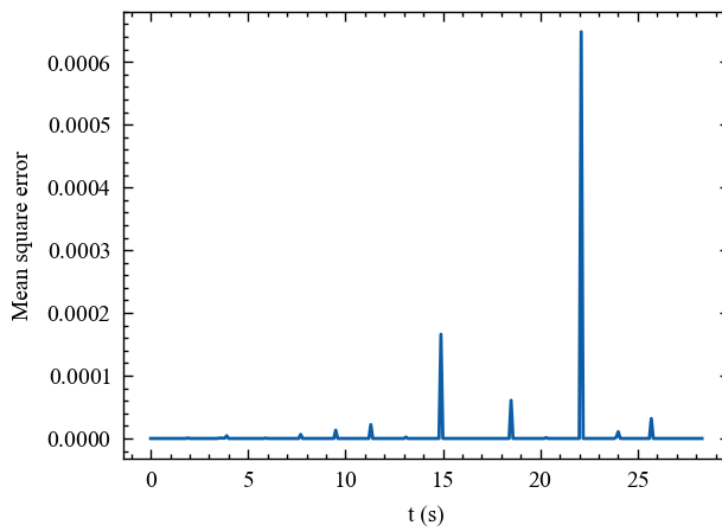


Figure 9 Mean square error of data at different times

Figure 9 displays the mean square error over time. It has been observed that at particular instances, the error shows a sudden increase, which may be due to the nonlinearity of the system. However, the overall error remains manageable, indicating that the results obtained from the DMD decomposition can accurately portray the characteristics of the flow field.

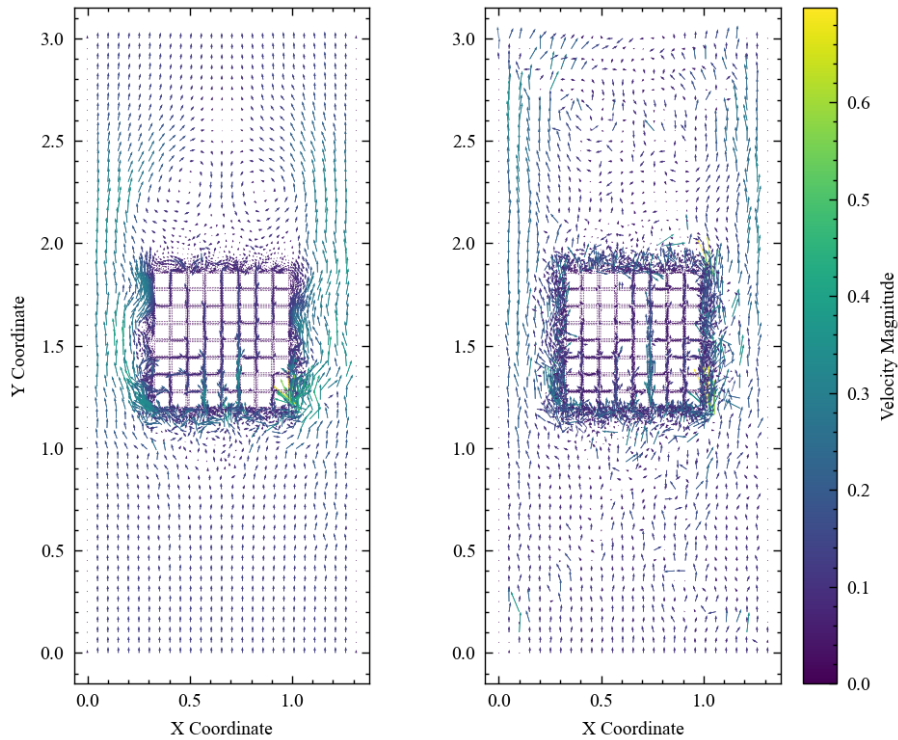


Figure 10 Velocity vector decomposed by DMD($t=10$ s)

Figure 10 shows the Velocity vector decomposed by DMD. The prediction effect at the 10th second is relatively good, and the vortex is successfully simulated. However, the position and size of the vortex are somewhat different from the CFD calculation and can be further optimized.

Results of POD

Figure 11 shows the Velocity vector decomposed by POD. Figure 12 shows the sum of the energy accounted for by the first 20 orders in the total energy. It can be found that the first 20 levels cannot express all energy.

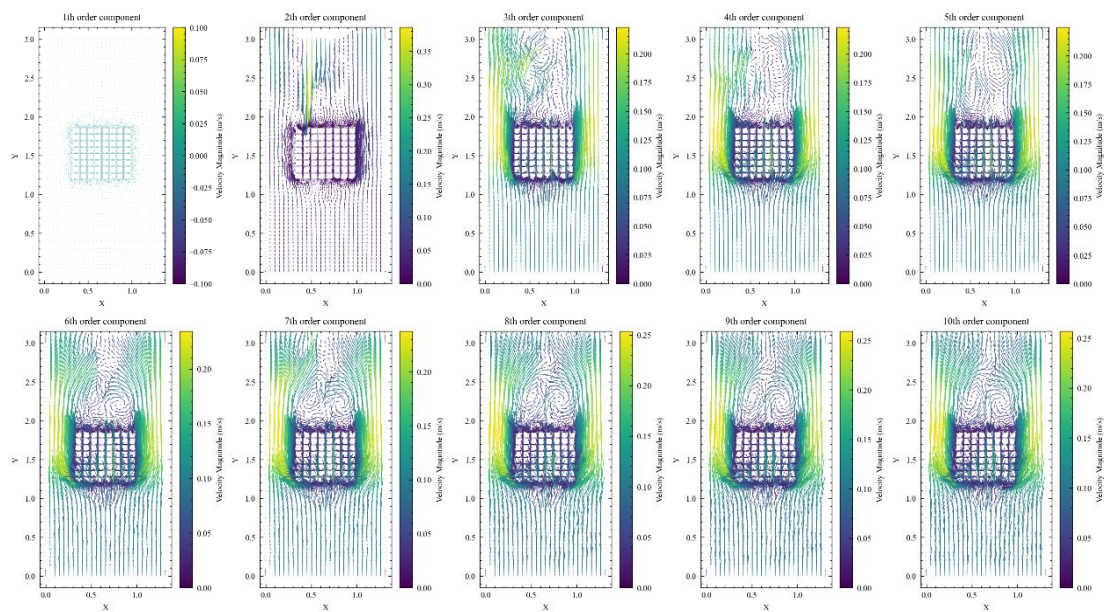


Figure 11 Velocity vector decomposed by POD($t=10$ s)

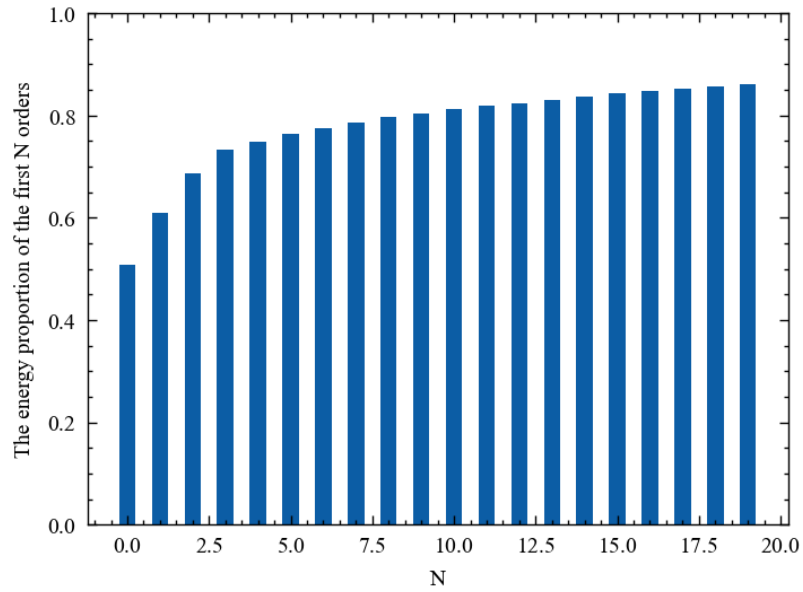


Figure 12 The sum of the energy accounted for by the first 20 orders

Figure 13 shows pressure field decomposed by POD at 10 s. It can be found that the POD algorithm is not very accurate when decomposing this flow field.

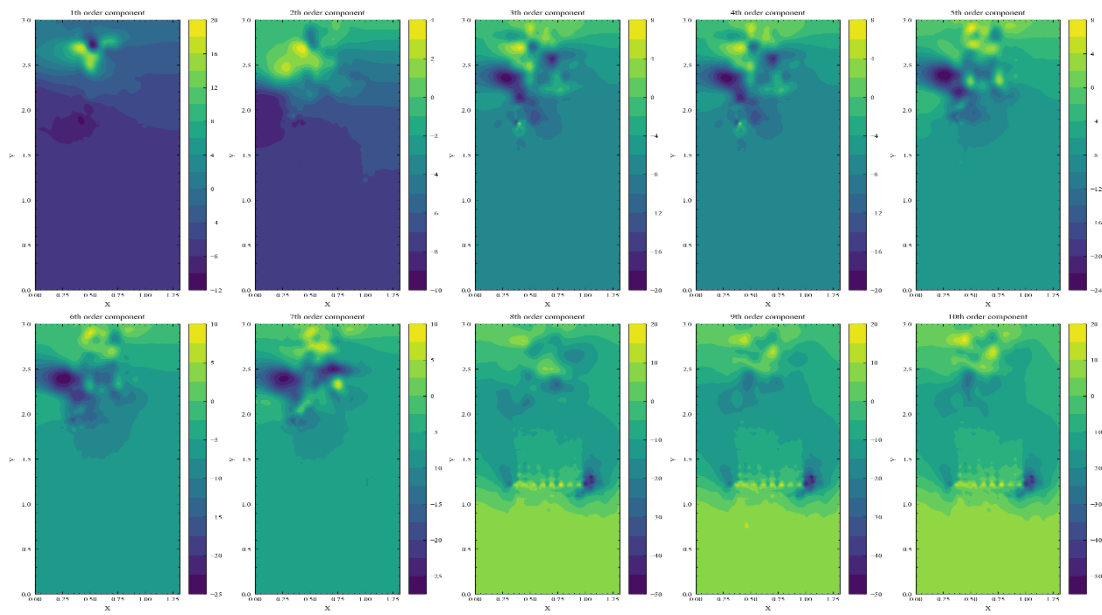


Figure 13 Pressure field decomposed by POD(t=10 s)

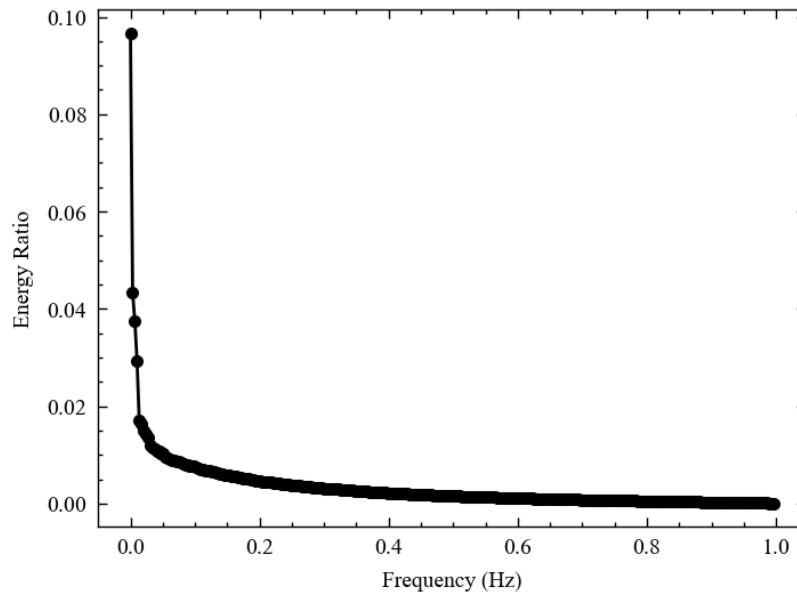


Figure 14 The proportion of energy each frequency by POD

Figure 14 shows the proportion of energy each frequency. It can be found that the main energy is mostly concentrated below 1Hz, which is different with results of DMD.

CONCLUSIONS

After CFD calculations, we found that vortex shedding will occur when flowing through the porous grid, and the vortex shedding is complicated. After the flow field decomposition of DMD and POD, we obtained the flow field characteristics of different orders, which provided an important basis for the mode identification of the flow field. Especially in the flow field after POD decomposition, obvious pressure oscillations can be found. There are many modes of oscillation, and the first 20 orders cannot accurately represent the energy in the flow field. In the DMD flow field decomposition and prediction, it is found that at certain moments, the covariance will suddenly increase, which should be related to nonlinear phenomena, and can be improved in the future.

REFERENCES

- Buongiorno, J., Jurewicz, J., Golay, M., & Todreas, N. (2016). *The offshore floating nuclear plant concept*. Nuclear Technology, 194(1), 1-14.
- Jurewicz, J. M. (2015). *Design and construction of an offshore floating nuclear power plant* (Doctoral dissertation, Massachusetts Institute of Technology).
- Zhang, Y., Buongiorno, J., Golay, M., & Todreas, N. (2018). Safety analysis of a 300-MW (electric) offshore floating nuclear power plant in marine environment. Nuclear Technology, 203(2), 129-145.
- Ma, Y., Zhang, J., Wang, M., Tian, W., Chen, R., Wu, Y., ... & Qiu, S. (2021). *Performance analysis of PRHRS in primary and secondary circuit for offshore floating nuclear plant*. Annals of Nuclear Energy, 164, 108580.
- Li, R., Peng, M., Xia, G., & Sun, L. (2020). The natural circulation flow characteristic of the core in floating nuclear power plant in rolling motion. Annals of Nuclear Energy, 142, 107385.